Solvent dependent and independent motions of CO–horseradish peroxidase examined by infrared spectroscopy and molecular dynamics calculations

Andras D. Kaposi[a], Ninad V. Prabhu[b], Sergio D. Dalosto[b], Kim A. Sharp[b], W.W. Wright[b], Solomon S. Stavrov[c], J.M. Vanderkooi[b],*

[a]*Department of Biophysics and Radiation Biology, Semmelweis University, Puskin u. 9, Budapest H-1088, Hungary*
[b]*Johnson Research Foundation, Department of Biochemistry and Biophysics, University of Pennsylvania School of Medicine, Philadelphia, PA 19104-6059, USA*
[c]*Sackler Institute of Molecular Medicine, Sackler School of Medicine, Tel Aviv University, Ramat Aviv, P.O. Box 39040, Tel Aviv 69978, Israel*

Abstract

The role of the solvent matrix in affecting CO bound to ferrous horseradish peroxidase was examined by comparing band-widths of ν_{CO} for the protein in aqueous solutions and in trehalose/sucrose glasses. We have previously observed that the optical absorption band and the CO stretching mode respond to the glass transition of glycerol/water in ways that depend upon the presence of substrate (Biochemistry 40 (2001) 3483). It is now demonstrated that the CO group band-width for the protein with bound inhibitor benzhydroxamic acid is relatively insensitive to temperature or the glass transition of the solvent. In contrast, in the absence of inhibitor, the band-width varies with the temperature that the glass is formed. The results show that solvent dependent and independent motions can be distinguished, and that the presence of substrate changes the protein such that the Fe–CO site is occluded from the solvent conditions. Molecular dynamic calculations, based upon X-ray structures, showed that the presence of benzhydroxamic acid decreases the distance between His42 and Arg38 and this leads for closer distances to the O of the CO from these residues. These results are invoked to account for the observed line width changes of the CO band.
© 2003 Elsevier Science B.V. All rights reserved.

*Corresponding author. Tel: +1-215-898-8783.
E-mail address: vanderko@mail.med.upenn.edu (J.M. Vanderkooi).

1. Introduction

Many enzymes carry out reactions with great precision at sites sequestered from water. At the same time, the active site must be accessible to the surface, since water-soluble reactants must bind and products must be released from the active site. Protein dynamics are recognized to play a role in reconciling the dichotomy between the need of access of water-soluble substrates and a sequestered active site. The effect of dynamics has been especially well studied for the CO derivative of the oxygen-binding hemoprotein, myoglobin. Here, photo-dissociation and the kinetics of recombination gave rise to the concept of dynamically-interconverting conformational substates [1]. Experimental differences in CO stretch frequencies are observed in homologous proteins, single-mutant derivatives of proteins and in varying external electric fields [22,27,29], features that led to the acceptance of the sensitivity of the CO infrared (IR) band as a marker of environment and dynamics of the protein.

The results of studies using myoglobin can be applied to examine heme enzymes, where the heme pockets are necessarily more intricate since reactions are catalyzed at the heme. To study the relationship between an enzyme's active site and the binding of a substrate we are examining the CO absorption band in the protein ferrous horseradish peroxidase (HRP). The frequency of CO bound to Fe(II) HRP is sensitive to the presence of the competitive inhibitor benzohydroxamic acid (BHA) and the protonation state of neighbouring groups [2,7,19].

In this study we are primarily concerned with the effect of solvent in influencing the internal ligand CO. It has previously been shown that the optical heme absorption band and the IR ν_{CO} band have widths that show temperature dependencies that are sensitive to the presence of substrate and the solvent glass transition [20]. Yet, the relationship between solvent viscosity, the sample temperature and the conformational heterogeneity of CO bound to the heme Fe remains unclear. For the purpose of seeing how the solvent affects the internal chromophore we are examing the protein incorporated into glasses formed at different tem-

peratures. Such glasses can be made from sugars, where the glass is formed as water evaporates from the sugar solution. Of the various sugars, trehalose is uniquely used in nature as a protector of protein under dehydrating conditions [5]. It has been used to study the effect of the matrix on the dynamics of heme proteins [13,15,30]. In preparing pure trehalose glasses microcrystals tend to form when the glass is prepared at low or ambient temperature. Making mixed sugar glasses can circumvent crystallisation [32]. In this way stable glasses can be formed at many different temperatures. This procedure was used in analysis of optical band width of cytochrome *c*, to distinguish contributions to the inhomogeneous distribution from solvent dependent and independent motions [30]. We here show that the sensitivity of the CO to the solvent depends upon the presence of the competitive inhibitor BHA and the pH. Molecular dynamics simulations help to understand these effects.

2. Materials and methods

2.1. Materials

Water was deionized and then glass distilled. Na dithionite and HRP type III (i.e. type C) was obtained from Sigma Chemical Co. (St. Louis MO). HRP was purified as described in Ref. [19] based upon the procedure of Paul [28]. The CO derivative of HRP was prepared as follows. Lyophilised HRP (7 mg) was added to 300 μl of the appropriate solution, placed in a 25-ml round bottom boiling vessel to which a vertical extension with an offset loop containing solid Na dithionite (5 mg) had been added. The solution for the glass was 300 mg trehalose, 300 mg sucrose and 500 μl water, which was heated to ∼60–64 °C until the sugars were fully dissolved. The aqueous solution was 60/40% v/v glycerol/aqueous buffer. The buffer for pH 6 was 20 mM K phosphate. For pH >9, 20 mM CAPSO was the buffer. The vessel was attached to a vacuum source and aspirated to remove dissolved gases. After 15 min, the valve on the vessel was closed. The vessel was removed from the vacuum and CO at 8–10 psi was introduced through the valve. After 15 min, Na dithionite was introduced to the solution and

mixed by swirling. The solution became bright orange–red. After retaining the CO atmosphere for 1.5 h, the vessel was opened. For the sample containing BHA, at this point BHA was added. The sample was immediately placed onto a 25.4 mm diameter$\times$2-mm thick quartz or CaF_2 disk. For the trehalose/sucrose glass samples made at 64 °C, the disk was placed on a hot plate at 64 °C for ~2 h until dry. In the trehalose/sucrose glass sample made at -20 °C the water was removed by placing the sample in a -20 °C refrigerator for 48 h. The CO remained bound under these conditions, as evident by the optical absorption spectrum.

2.2. Spectroscopy

IR spectra were obtained with a Bruker IFS 66 Fourier transform IR instrument (Bruker, Brookline, MA) as described by Kaposi et al. [19]. A Hitachi Perkin–Elmer absorption instrument was used to take the visible absorption spectra. For both instruments, a transmission cell holder with a 100 μm spacer and CaF_2 windows was used to hold the sample. The temperature of the sample was regulated by a top-loading OmniPlex cryostat (APD Cryogenics, Allentown, PA). The spectra were obtained in the sequence of high temperature to low temperature at 10° increments starting at 290 K. The rate of cooling was approximately 1° min^{-1}. The lowest temperature obtained was 11–13 K.

2.3. Analysis of spectral bands

The method of moments was used to describe band positions and widths [23,26] and also used to characterize CO-HRP [20].

M_0 is a value describing the intensity of the band. The first moment is the center of the band:

$$M_1 = \frac{1}{M_0} \int \omega F(\omega) d\omega$$

where ω is the frequency and $F(\omega)$ is the absorbance. The width of the band determines the second moment, M_2:

$$M_2 = \frac{1}{M_0} \int \omega^2 F(\omega) d\omega - M_1^2$$

In case of a Gaussian band, the connection between the full width at half maximum (FWHM) and M_2 is the following:

$$M_2 = \frac{(\text{FWHM})^2}{8 \ln 2}$$

The PEAKFIT™ program used for Gaussian fits produced the sigma parameter of the width. FWHM was calculated from the sigma: FWHM = 2.3548 sigma.

2.4. Molecular dynamics

Dynamics simulations were run using the CHARMM 27 program suite [3]. The force field for the molecular dynamics simulations of HRPC was the CHARMM 22 all atom parameter set [25] and the starting structures were 1ATJ [12] or 2ATJ [16] (PROTEIN data base) for the protein without or with BHA, respectively. Due to the absence of force field parameters for BHA in CHARMM 22 we have derived parameters from BHA coordinates taken from the 2ATJ entry using ab initio quantum mechanical calculations as follows. The hydrogens were added using CHARMM and energy minimization was done to remove bad contacts. Charges were calculated using the Hartree Fock method used in the GAUSSIAN program. Bond stretch, angle and torsion parameters were borrowed from analogous atom types in the CHARMM potential. The values and atom types are listed in Table 1.

The solvent was modeled as a continuum by incorporating the solvent contribution to the free energy from the solution of the Poisson–Boltzmann equation using the program ZAP. ZAP parameters used a dielectric of 80 for the solvent. A hydrophobic coefficient of 6 cal $(\text{mol A})^{-1}$ was used in the solvent accessible surface area model to obtain the apolar contributions to the free energy [14]. This continuum solvent model reduces the computational time since a system of the size of HRPC in a box of explicit solvent with periodic boundary conditions would contain greater than

Table 1
Parameters for BHA

Atom name	CHARMM atom type	Charge
C	CC	0.512
O1	OC	−0.650
N	NH_2	−0.341
NH	H	0.274
O2	OC	−0.574
C1	CA	0.081
C2	CA	−0.081
H2	HP	0.092
C6	CA	−0.144
H6	HP	0.083
C3	CA	−0.142
H3	HP	0.079
C5	CA	−0.140
H5	HP	0.089
C6	CA	−0.170
H6	HP	0.137

The table contains the assigned CHARMM atom types and partial charges for the BHA atoms. The heavy atom names correspond to the nomenclature in 2ATJ PDB. The hydrogens were added by CHARMM and the atom names reflect the heavy atom to which they are bound. The partial charges were calculated by ab initio methods described in the text.

40 000 atoms. All alpha carbons, the BHA atoms, and the two Ca^{2+} ions were restrained by a force of 24 kcal mol^{-1} A^{-2} to ensure the overall stability of the protein structure during the course of the simulations and all bond lengths were constrained by SHAKE. The dihedral angles on the substituent group on the phenyl ring of BHA, except around the N–O_2 bond, were harmonically restrained by a force constant of 50 kcal mol^{-1} to angles corresponding to the PDB coordinates. The effect of N–O_2 bond rotation was examined, as indicated in Fig. 1. We used density functional theory, B3LYP/6-31G* functional and basis sets to determine the energy surface. As seen in the figure, the resulting potential energy surface indicates that there are two energy wells, of which one is strongly preferred, hence justifying the harmonic restraint.

Other MD simulations show that the side chain atoms give rise to most of the dynamical deviations in protein [4]. Comparison of this protocol (with ZAP and similar constraints) with explicit water in a MD simulation of a smaller protein, calmo-

dulin (with restraints), will be published elsewhere (Prabhu and Sharp, personal communication).

In the four simulations presented here, the water bound inside the protein seen in the 1ATJ and 2ATJ PDB files is replaced by CO. One simulation, based upon 1ATJ, has His42 positively charged with hydrogen atom attached to the nitrogen N_ε. The second simulation had this hydrogen removed so that His42 was neutral. The third and fourth simulations, based upon 2ATJ, include BHA, with the same charges as first and second simulations, respectively. The determination of the positions of the atoms of BHA is given in the appendix. All structures were first energy minimized and, after short heating and equilibration, the simulations were run for 500 ps. The structures were saved
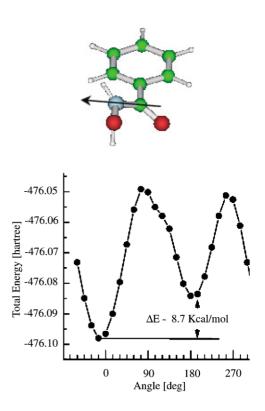

Fig. 1. Optimization of BHA. The potential surface along the dihedral angle formed by C–N is shown. This angle was rotated in steps of 15° and letting the structure relax using Hartree Fock method from the GAUSSIAN program. The structure of BHA is shown in the inset. The coordinates of the heavy atoms were taken from 2ATJ PDB data file. The hydrogens were constructed using CHARMM.

every 0.1 ps for analysis The purpose of these simulations, given the approximations employed, are limited to the examination of side chain motions in the interior of the protein that are not accompanied by large main chain rearrangements. An estimation of the electric field at the O of the C–O bond used the CHARMM partial charges that were assigned to the atomic coordinates in each snap-shot of the trajectory. Coulomb's law with the principle of superposition was used to calculate the field. The protein dielectric was estimated to be 1.

3. Results

3.1. IR spectra

The IR absorption bands of CO bound to HRP were examined under various medium conditions. Examples of spectra are shown in Fig. 2. In Fig. 2a and b we compare the CO stretching band for the ferrous HRP–BHA complex in the sugar glass formed at −20 and 64 °C, respectively. The band position is at 1915 cm^{-1} at 293 K for both samples. The absorption maxima for both samples shift to higher frequency as temperature decreases. The sample prepared in the sugar glass at 64 °C is wider over the whole temperature range. In Fig. 2c the CO stretching band for ferrous HRP complex without BHA in the sugar glass is shown. In the absence of the competitive inhibitor the band-width is considerably wider than in its presence (Fig. 2a and b).

It can be noted that the band consists of more than one peak (at least three). Because the peaks of the HRP–BHA complex were not rigorously single, a fitting procedure was used to analyze position and width. Examples of the fits are shown on Fig. 3. The fitting confirms the observation noted above that the width of the CO band for the sample in glass formed at high temperature is broader than for the sample in glass formed at lower temperature. Multiple peaks were also observed by Holzbaur et al. [17], and are attributed to different conformers. For our further analysis we considered the major peak. The wide Gaussian component corresponds to the trehalose/sucrose background measured at the same temperature.

The positions of the major peaks, expressed as first moments, are shown as a function of temperature on Fig. 4. The general trend is lower frequency as temperature increases.

3.2. CO band widths

The widths of the major peaks are depicted on Fig. 5, as the second moment. In the samples with BHA the width changes less than 50% over the approximately 300 K temperature range. The width in the glass formed at higher temperature is wider over the whole temperature range compared to the glass formed at lower temperature. The width of CO band for the BHA–HRP complex in glycerol/water is in between the two sugar glasses in the same temperature range.

Samples without the substrate analogue BHA were measured in three different conditions and the band-widths, expressed as a second moment, are also shown in Fig. 5. In contrast to the BHA bound protein, the widths of the ν_{CO} band in the absence of BHA are dramatically influenced by solvent conditions. In glycerol/water at pH 6 the value of M_2 was 50 cm^{-2} (16.7 cm^{-1} FWHM) at the highest temperature and decreased to less than 10 cm^{-2} (7.5 cm^{-1} FWHM) at the glass transition (170 K). For trehalose glass formed at 64 °C the M_2 width is 35 cm^{-2} (13.9 cm^{-1} FWHM) and the width decreases gradually to 20 cm^{-2} (10.6 cm^{-1} FWHM) at 14 K. Therefore, the sample where the glass was formed at high temperature remains broad at low temperature, which we interpret to mean that the fluctuations that occur at high temperature are frozen in. Therefore, the band width for CO in the sample without BHA is a function of the inhomogeneous distribution achieved at high temperature.

A second perturbation was to compare the sample at lower (pH 6) and higher pH (9.3). These experiments were carried out without BHA. At higher pH the width is considerably narrower than for low pH above the glass transition and the sample shows less dependence upon solvent.

3.3. Molecular dynamics

In order to get some insight on the effect of BHA binding and pH change, a molecular dynam-
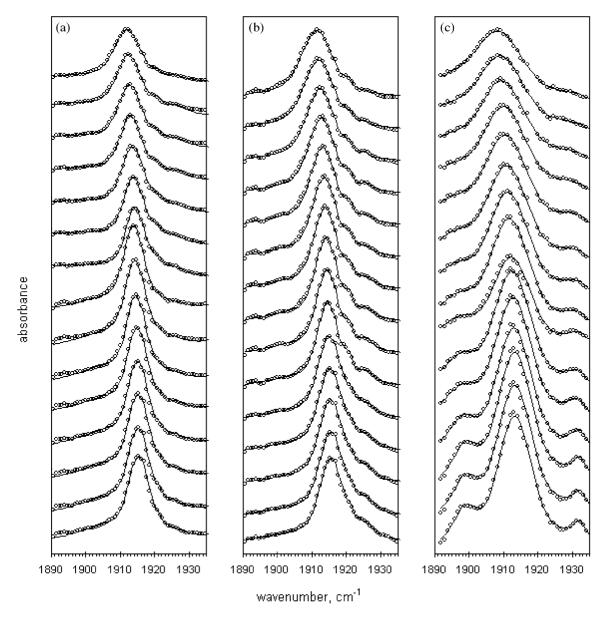
Fig. 2. IR absorption spectra of CO–HRP–BHA complex in trehalose/sucrose film prepared at −20 °C (a) and prepared at 64 °C (b), and CO–HRP in trehalose prepared at 64 °C (c), stacked plot. The pH was ∼6. Measuring temperature from top to bottom: 290, 270,…, 50, 30, 14 K. Solid line: fitted curve, symbols: data points. For clarity we show only every second data point.

ics simulation of the CO-protein was carried out. For reference, the heme, Arg38 and His42 and BHA are shown in Fig. 6. CO, in yellow, is also shown.

The root mean square deviation (RMSD) for each residue of the entire protein is shown in Fig. 7a and b without BHA. Fig. 7c and d are with BHA. Binding substrate and adding or removing
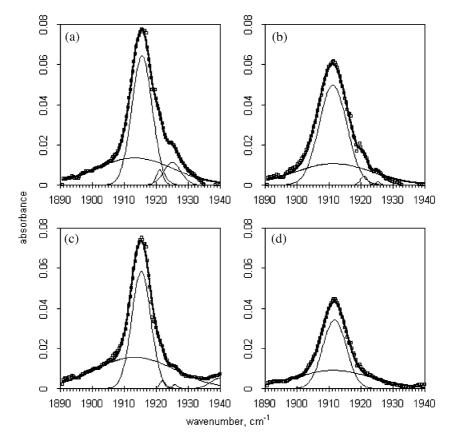
Fig. 3. Measured IR spectra and fitting examples of CO–HRP–BHA complex in trehalose/sucrose film. Upper panels (a and b): sample prepared at 64 °C, lower panels (c and d): sample prepared at −20 °C. Left panels (a and c): measuring temperature: 14 K, right panels (b and d): measuring temperature: 295 K.

an hydrogen on His42 changes the RMSD of residues throughout the protein. In Fig. 7a and c the distal His42 is protonated (low pH case) while in b and d His42 is deprotonated (high pH case). The residues showing the largest RMSD are generally those that are on the surface; for instance Lys149 and Asp150, or those residues that are in the flexible channel Phe142 and Phe143. The amplitudes of the RMSD of individual residues are seen to vary depending on the simulation conditions. Some residues, for example, Phe68, show lower RMSD in the presence of BHA. Residues like Arg178 show higher RMSD in the presence of BHA relative to the absence of BHA in the higher pH case. Phe68, Gln128, Arg264 and

Leu299 at high pH have RMSD that are approximately ∼1 A larger than the values at low pH. This shows that there are large mean displacements at high pH. Phe142, Asn154 and Asp282 show larger standard deviations in the RMSD at higher pH. This shows larger mean fluctuations at high pH. These differences in the positions and fluctuations of the residues on changing the pH conditions or the presence of BHA may result in differences in the resultant electric field at CO.

The residues near the CO are the most important in affecting the frequency, because interactions fall off steeply with increasing distance. Arg38 and His42 are in the heme pocket, with Arg38 serving to stabilize the peroxy complex [24]. These resi-
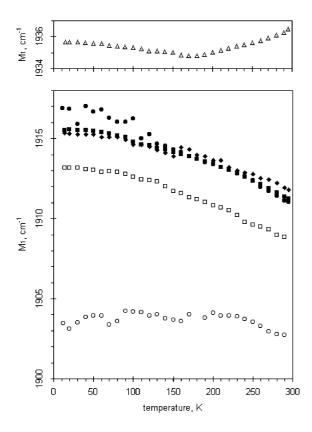
Fig. 4. Temperature dependence of the first moments of the IR CO absorption band. CO–HRP in trehalose film sample prepared at 64 °C (open square). CO–HRP–BHA complex in trehalose/sucrose film; sample prepared at −20 °C (filled diamond) and at 64 °C (filled square). CO–HRP in glycerol/water at pH 6 (open circle), CO–HRP–BHA complex in glycerol/water at pH 6 (closed circle), CO–HRP in glycerol/water at pH 9.3 (open triangle). Note that filled symbols are used for cases when substrate (BHA) is added and quadrilateral symbols (square and diamond) are used for cases when matrix is trehalose or trehalose/sucrose mixture.

dues are shown by recent quantum treatment using Density Functional Theory to interact with bound CO in peroxidase model clusters [6]. As seen in Fig. 7, these residues exhibit relatively low RMSD values, but since they are close to the CO, any motion that would be expected to result in changes in distance to the CO will produce broadening of the band [6]. While the consequences of motion upon the CO band awaits quantum calculations, at the level of molecular mechanics a qualitative

understanding of the effects of substrate bonding on distances and mobility can be achieved. Distances between residues are examined in Fig. 8 without BHA and in Fig. 9 with BHA. As in Fig. 7, the case for His42 protonated at the N_ε (considered to correspond experimentally to low pH, [8]) and this position deprotonated (considered to correspond experimentally to high pH) were also examined. Three distances are plotted as a function of time: Arg38–His42 (dashed), His42–O (dotted) and Arg38–O (solid), where O belongs to CO. Raising pH reduces the positive charge on His; in this case the distance between His42 and Arg38 becomes closer, as would be intuitively predicted based upon the charge. The presence of BHA also decreases the Arg–His distance (com-
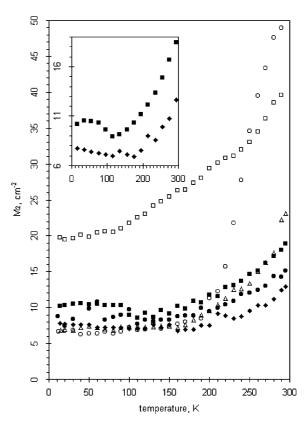

Fig. 5. Temperature dependence of the second moments of the IR CO absorption band. For symbols used, see legend of Fig. 4.
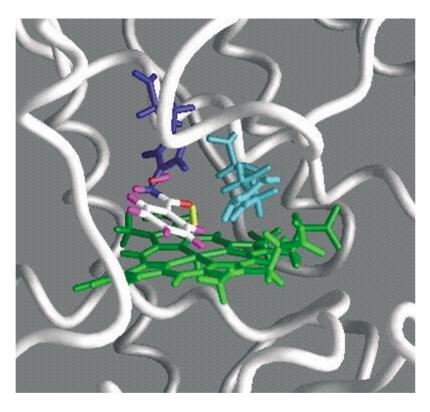
Fig. 6. Picture of the heme pocket. Heme is green, BHA is white, His38 is blue and Arg42 is turquoise.

pare Figs. 8 and 9 upper). It also decreases the Arg–O distance while the His–O distance remains about the same. The CO frequency is certainly influenced by both His and the positively charged Arg. In comparing Panel 8 upper and 8 lower, upon removing a proton from His, which in experiment is the same as raising the pH, the distances for the $^{Arg}N_{\varepsilon}\cdots O^{co}$ (solid line) increase and $^{his42}N_{\varepsilon}\cdots O^{co}$ (dotted line) decreases. The decreases in distance would be consistent with a more defined structure, resulting in sharper IR bands. Note that His–Arg distance seems to fluctuate between two equilibrium positions. This behavior would be expected if there is a fast dynamic equilibration between protein substates, such that there is rotation of the imidazole moity. The $^{His42}N_{\varepsilon}-O^{CO}$ distance does not change. However, in the low pH case, H_{ε} is present, causing the His42 to be closer to CO.

BHA binds tightly to the protein in a specific binding site [16]. In the next figure, the effect of BHA on RMSD was examined as a function of distance from the heme site. Fig. 10a shows that the RMSD are larger as distance from heme increases. Also as expected the area of residues exposed to solvent increases as distance from heme increases (Fig. 10b). In the inset, it can be seen that there is a significant decrease in water exposure for the closest residues when BHA binds.

The final calculation that was carried out was to evaluate the electric field along the CO band for each of the dynamical structures. Fig. 11 shows the populations of MD snap-shots against the calculated electric field along the CO bond. BHA shifts the center of the distribution to a value in between high and low pH simulation in complete agreement with the experiment. In other words, the field progresses in this series: no substrate low
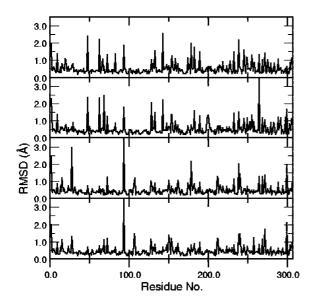
Fig. 7. RMSD as a function of residue. The RMSD were calculated for each residue and averaged over the whole MD trajectory. From top to bottom: His42 is protonated, no BHA; His42 is unprotonated, no BHA; His42 is protonated, BHA present; His42 is unprotonated, BHA present.

pH <substrate low pH <high pH. This same sequence gave a CO frequency of 1904, 1911 and 1934 cm^{-1}, respectively.

4. Discussion

The current thinking about protein dynamics is that at high temperature there is a wide distribution of conformations, arising from diffusive motions of secondary structure. As the temperature decreases, the protein relaxes to lower energy states. However, since the solvent influences motion, when the solvent forms a glass, conformations of the protein arising from large-scale motions are 'frozen in' due to the enormous increase in viscosity at the glass transition. The ensemble of molecules is now distributed into a variety of conformations that reflect the distribution of sub-conformations that exist at the glass transition temperature.

In an ideal case where the inhomogeneous linewidths are narrow, the experimental spectral line widths for condensed phases would be a measure

of fluctuations [25]. However, for proteins the disorder and viscosity of the solvent may not uniformly influence the disorder of specific markers and residues of the protein. Small internal fluctuations, such as those sensitively measured by resolved spectral hole-burning experiments [11,31,33], will still occur at temperatures below the glass transition. But the larger motions that require solvent displacement will not occur at temperatures below the solvent glass transition since the sub-conformations can inter-convert only very slowly due to a high-energy barrier imposed by the rigid solvent. Analysis of spectral lines as a function of temperature can reveal the existence
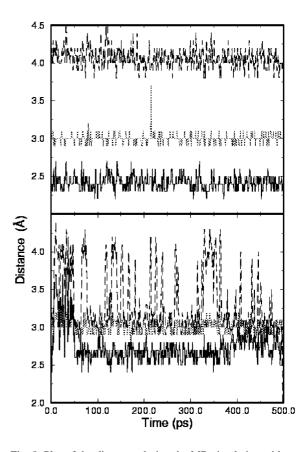

Fig. 8. Plot of the distances during the MD simulation without BHA. Upper panel, distances for the $^{Arg}H_\varepsilon \cdots O^{oc}$ (solid line), $^{his}N_\varepsilon \cdots O^{oc}$ (dotted line) and $^{his}N_\varepsilon \cdots ^{Arg}H_1$ (dashed line) with the distal His42 protonated. Lower panel shows the distances $^{Arg}H_\varepsilon \cdots O^{oc}$ (solid line), $^{his}N_\varepsilon \cdots O^{oc}$ (dotted line) $^{his}N_\varepsilon \cdots ^{Arg}H_1$ (dashed line) with the distal His42 unprotonated.
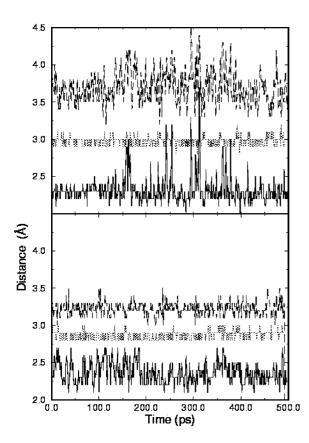
Fig. 9. Plot of the distances during the MD simulation with BHA. Upper panel, distances for the $^{Arg}H_\varepsilon\cdots O^{oc}$ (solid line), $^{his}N_\varepsilon\cdots O^{oc}$ (dotted line) and $^{his}N_\varepsilon\cdots^{Arg}H_1$ with the distal His42 protonated. Lower panel shows the distances $^{Arg}H_\varepsilon\cdots O^{oc}$ (solid line), $^{his}N_\varepsilon\cdots O^{oc}$ (dotted line) $^{his}N_\varepsilon\cdots^{Arg}H_1$ (dashed line) with the distal His42 unprotonated.

of fluctuations, but in practice, it is difficult to separate the diffusive motions depend upon the solvent from these other effects. As an experimental tool, it would be desirable to examine the protein where one has some means to control the disorder of the polypeptide chain. The approach taken in this work is to incorporate proteins in glasses that were formed at different temperatures, and then compare its properties over a range of temperatures.

The peak positions and line-widths of the CO stretch absorption band are influenced by changes in pH and addition of substrate. In discussing the results we refer to Fig. 6, showing the heme and

relevant amino acids. On the proximal side His170 is ligated to the iron and its positive charge allows a salt link to Asp247. For this reason, the solvent is less likely to cause major changes in the positions of the polypeptide chain on the proximal side. CO binds on the distal side, and BHA also binds adjacent to the heme on this side. The distal His42 and Arg38 acids are influential in determining ν_{CO} [6]. The main idea in the interpretation of the anharmonic temperature dependence of the IR bandwidths is that heating populates higher-energy conformations that are much more flexible than the lowest-energy conformation. One can imagine that in the higher-energy conformation one or
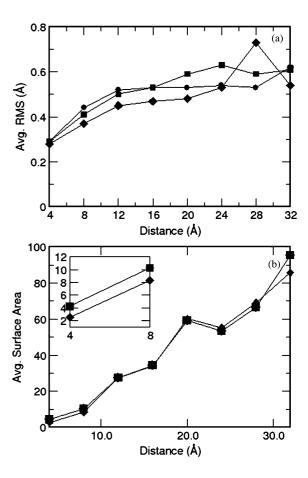

Fig. 10. Effect of distance from heme on residue behaviour. Circles: no BHA, His protonated. Squares: BHA, His protonated. Diamonds: no BHA, His deprotonated. (a) RMS vs. distance. (b) Surface area vs. distance.
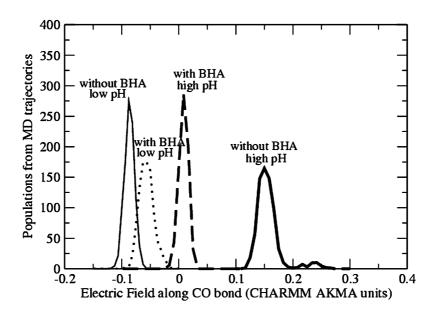
Fig. 11. Population of MD snap-shots corresponding to the electric field along the CO bond for complexes indicated. The bin size was 0.00625 AKMA units.

several hydrogen bonds, which anchor an amino acid or some amino acids in the lowest energy conformation, are broken.

The straight-forward way to change the dynamics of the protein is to change the temperature. H bonding strength decreases with increase in temperature [18]. The IR amide I′ band absorption of HRP shows that the protein retains its overall secondary structure over a temperature range of ∼300°, from room temperature to 10 K and that the substrate of HRP remains bound to protein at low temperature [9,10]. But there are changes in the protein as H bonding between the solvent molecules and the exposed amide bonds become stronger at lower temperature, seen in changes in the amide I′ band position and strength [19].

We consider first the case without BHA. In this situation, changing the pH from 6.0 to 9.3 at room temperature markedly reduces the line width. When temperature is decreased, the width seen at pH 6.0 narrows relatively more than the higher pH case, so that at low temperature both have approximately the same line-width. At pH 6.0 the width is markedly affected by trehalose. At high temperature the width is broad both in trehalose glass

formed at 60 °C and in glycerol/water (the somewhat narrower width in trehalose glass may indicate that trehalose is preventing the large-scale motions). At lower temperatures, the effect of the glass is most noticeable. At temperatures lower than 200 K, the width of the line is more than twice that for the same in glycerol/water glass. The interpretation that is in the presence of the glass system has been trapped in the higher energy states, and consequently, the band remains broad.

The addition of BHA has a profound effect on the line-width of ν_{CO}. Under all medium conditions, BHA reduces the width. The width narrows as temperature decreases, and the widths are narrowest when the glass was formed at low temperature, but the effect of the glass is much less pronounced than in its absence. We again to go to the structure for an explanation. BHA hydrogen bonds to Arg38, Pro139 and His42 [16]. The simulations (Fig. 9) indicate that the distances between Arg and CO are reduced, relative to its absence. The simulation indicates that BHA reduces fluctuations in the amino acids neighbouring the bound CO. In this model, the substrate analogue is influencing the isolation of CO from the

solvent. The reaction mechanism of HRP is in effect sequential—first the binding of the water soluble H_2O_2 and then the binding of the aromatic substrate. The binding of the substrate changes the heme pocket, making it much more rigid, as indicated by the marker CO. The closed flap in BHA case would trap solvent inside whereas in the non-BHA case, the open flap would allow solvent exchange with the bulk, enhance mobility of water and hence possibly broadening of the spectrum. We suggest that this change in dynamics contributes to the specificity of the catalytic reaction. Khajehpour et al. [21] using phosphorescence quenching, have shown that oxygen accessibility to the heme pocket is influenced by BHA.

To summarize, the presence of substrate has a large effect on the sensitivity of the bound ligand to changes in the solvent. In the absence of BHA, the line width of CO is sensitive to the dynamics of the solvent since the width follows the glass transition of glycerol/water, and it remains broad at low temperature when it is incorporated in a trehalose/sucrose glass formed at high temperature. In contrast, in the presence of BHA, the interior is very little dependent upon the exterior viscosity, indicating that BHA has caused a change in the protein so that the residues around the heme have occluded solvent effects.

Acknowledgments

References

[1] R.H. Austin, K.W. Beeson, L. Eisenstein, H. Frauenfelder, I.C. Gunsalus, Dynamics of ligand binding to myoglobin, Biochemistry 14 (1975) 5355–5373.

[2] C.H. Barlow, P.-I. Ohlsson, K.-G. Paul, Infrared spectroscopic studies of carbonyl horseradish peroxidases, Biochemistry 15 (1976) 2225–2229.

[3] B.R. Brooks, R.E. Bruccoleri, B.D. Olafson, D.J. States, S. Swaminathan, M. Karplus, CHARMM: a program for macromolecular energy minimization and dynamics calculation, J. Comp. Chem. 4 (1983) 187–217.

[4] G. Cottone, L. Cordone, G. Ciccotti, Molecular dynamics simulation of carboxy-myoglobin embedded in a trehalose–water matrix, Biophys. J. 80 (2001) 931–938.

[5] L.M. Crowe, D.S. Reid, J.H. Crowe, Is trehalose special for preserving dry biomaterials?, Biophys. J. 71 (1996) 2087–2093.

[6] S.D. Dalosto, N.V. Prabhu, J.M. Vanderkooi, K.A. Sharp, A density functional theory study of conformers of the ferrous CO complex of horseradish peroxidase with distinct Fe–C–O configurations, J. Phys. Chem. B 107 (2003) (1884) 1892.

[7] R. Evangelista-Kirkup, G. Smulevich, T.G. Spiro, Alternative carbon monoxide binding modes for horseradish peroxidase studied by resonance Raman spectroscopy, Biochemistry 25 (1986) 4420–4425.

[8] A. Feis, J.N. Rodriguez-Lopez, R.N.F. Thorneley, G. Smulevich, The distal cavity structure of carbonyl horseradish peroxidase as probed by the resonance Raman spectra of His 42 and Arg 38 Leu mutants, Biochemistry 57 (1998) 15575–15581.

[9] J. Fidy, G.R. Holtom, K.-G. Paul, J.M. Vanderkooi, The binding of napththohydroxamic acid to horseradish peroxidase monitored by Zn-mesoporphyrin fluorescence line narrowing, J. Phys. Chem. 95 (1991) 4364–4370.

[10] J. Fidy, K.-G. Paul, J.M. Vanderkooi, Differences in the binding of aromatic substrates to horseradish peroxidase revealed by fluorescence line narrowing, Biochemistry 28 (1989) 7531–7541.

[11] J. Gafert, C. Ober, K. Orth, J. Friedrich, Thermal broadening of an optical transition in a chromoprotein between 50 mK and 15 K, J. Phys. Chem. 99 (1995) 14561–14565.

[12] M. Gajhede, D.J. Schuller, A. Henriksen, A.T. Smith, T.L. Poulos, Crystal structure of horseradish peroxidase c at 2.15 A resolution, Nature Struct. Biol. 4 (1997) 1032–1038.

[13] D.S. Gottfried, E.S. Peterson, A.G. Sheikh, J. Wang, M. Yang, J.M. Friedman, Evidence for damped hemoglobin dynamics in a room temperature trehalose glass, J. Phys. Chem. 100 (1996) 12034–12042.

[14] J.A. Grant, B.T. Pickup, A. Nicholls, A smooth permittivity function for Poisson–Boltzmann solvation methods, J. Comp. Chem. 22 (2001) 608–640.

[15] S.J. Hagen, J. Hofrichter, W.A. Eaton, Protein reaction kinetics in a room-temperature glass, Science 269 (1995) 959–962.

[16] A. Henriksen, D.J. Schuller, K. Meno, K.G. Welinder, A.T. Smith, M. Gajhede, Structural interactions between horseradish peroxidase C and the substrate benzhydroxamic acid determined by X-ray crystallography, Biochemistry 37 (1998) 8054–8069.

[17] I.E. Holzbaur, A.M. English, A.A. Ismail, Infrared spectra of carbonyl horseradish peroxidase and its substrate complexes: characterization of pH-dependent conformers, J. Am. Chem. Soc. 118 (1996) 3354–3359.

[18] G.A. Jeffrey, An Introduction to Hydrogen Bonding, Oxford University Press, New York, 1997.

[19] A.D. Kaposi, J. Fidy, E.S. Manas, J.M. Vanderkooi, W.W. Wright, Horseradish peroxidase monitored by infrared spectroscopy: effect of temperature, substrate and calcium, Biochim. Biophys. Acta 1435 (1999) 41–50.

[20] A.D. Kaposi, J.M. Vanderkooi, W.W. Wright, J. Fidy, S.S. Stavrov, Influence of static and dynamic disorder on the visible and IR absorption spectra of carbonmonoxy horseradish peroxidase, Biophys. J. 81 (2001) 3472–3482.

[21] M. Khajehpour, T. Troxler, J.M. Vanderkooi, Effect of protein dynamics upon reactions that occur in the heme pocket of horseradish peroxidase, Biochemistry 42 (2003) 2672–2679.

[22] M. Laberge, J.M. Vanderkooi, K.A. Sharp, Effect of a protein electric field on the CO-stretch frequency. Finite difference Poisson–Boltzmann calculations on carbonmonoxy cytochromes *c*, J. Phys. Chem. 100 (1996) 10793–10801.

[23] M. Lax, The Franck–Condon principle and its application to crystals, J. Chem. Phys. 20 (1952) 1752–1760.

[24] H. Li, T.L. Poulos, Structural variation in heme enzymes: a comparative analysis of peroxidase and P450 crystal structures, Structure 2 (1994) 461–464.

[25] A.A. MacKerell Jr., M. Bashford, R.L. Bellott, et al., All-atom empirical potential for molecular modeling in dynamics studies of proteins, J. Phys. Chem. B. 102 (1998) 3586–3616.

[26] D.L. Orth, R.J. Mashl, J.L. Skinner, Optical lineshapes of impurities in crystals: a lattice model of inhomogeneous broadening by point defects, J. Phys.: Condensed Matter 5 (1993) 2533–2544.

[27] E.S. Park, S.S. Andrews, R.B. Hu, S.G. Boxer, Vibrational Stark spectroscopy in proteins: a probe and calibration for electrostatic fields, J. Phys. Chem. B 103 (1999) 9813–9817.

[28] K.-G. Paul, Die Isolierung von Meerrettichperoxidase, Acta Chem. Scand. 12 (1958) 1312–1318.

[29] G.N. Phillips Jr., M.L. Teodoro, T. Li, B. Smith, J.S. Olson, Bound CO is a molecular probe of electrostatic potential in the distal pocket of myoglobin, J. Phys. Chem. B 103 (1999) 8817–8829.

[30] N.V. Prabhu, S.D. Dalosto, K.A. Sharp, W.W. Wright, J.M. Vanderkooi, Optical spectra of Fe(II) cytochrome *c* interpreted using molecular dynamics simulations and quantum mechanical calculations, J. Phys. Chem. B. 106 (2002) 5561–5571.

[31] J. Schlicter, J. Friedrich, L. Herenyi, J. Fidy, Protein dynamics at low temperatures, J. Chem. Phys. 112 (2000) 1–10.

[32] W.W. Wright, J.C. Baez, J.M. Vanderkooi, Mixed trehalose/sucrose glasses used for protein incorporation as studied by IR and phosphorescence spectroscopy, Anal. Biochem. 307 (2002) 167–172.

[33] J. Zollfrank, J. Friedrich, J.M. Vanderkooi, J. Fidy, Conformational relaxation of a low temperature protein as probed by photochemical hole burning: horseradish peroxidase, Biophys. J. 59 (1991) 305–312.